Label-Free Analysis with Multiple Parameters Separates G Protein-Coupled Receptor Signaling Pathways

Suutari, Teemu; Rahman, Sabrina N.; Vischer, Henry F.; Van Iperen, Dick; Merivaara, Arto; Yliperttula, Marjo; Leurs, Rob; Kool, Jeroen; Viitala, Tapani

Link to publication in VU Research Portal

Label-Free Analysis with Multiple Parameters Separates G Protein-Coupled Receptor Signaling Pathways

Teemu Suutari,* Sabrina N. Rahman, Henry F. Vischer, Dick van Iperen, Arto Merivaara, Marjo Yliperttula, Rob Leurs, Jeroen Kool, and Tapani Viitala*

Read Online

ACCESS | Metrics & More | Article Recommendations | Supporting Information

ABSTRACT: Real-time label-free techniques are used to profile G protein-coupled receptor (GPCR) signaling pathways in living cells. However, interpreting the label-free signal responses is challenging, and previously reported methods do not reliably separate pathways from each other. In this study, a continuous angular-scanning surface plasmon resonance (SPR) technique is utilized for measuring label-free GPCR signal profiles. We show how the continuous angular-scanning ability, measuring up to nine real-time label-free parameters simultaneously, results in more information-rich label-free signal profiles for different GPCR pathways, providing a more accurate pathway separation. For this, we measured real-time full-angular SPR response curves for G_s, G_q, and G_i signaling pathways in living cells. By selecting two of the most prominent label-free parameters: the full SPR curve angular and intensity shifts, we present how this analysis approach can separate each of the three signaling pathways in a straightforward single-step analysis setup, without concurrent use of signal inhibitors or other response modulating compounds.
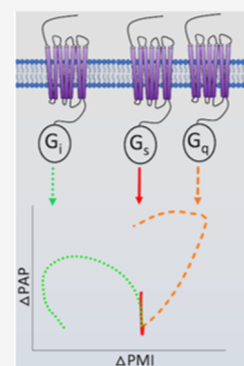
G protein-coupled receptors (GPCRs) are the largest family of transmembrane proteins. They are responsible for a number of physiological functions and, as such, play a crucial role in several diseases. Their importance is highlighted by the fact that 35% of all FDA approved drugs mediate their effect via GPCRs,[1] and they are still widely investigated for new drug targets as there are still hundreds of known receptors that are not targeted by any currently marketed drugs.[2] GPCRs are coupled to heterotrimeric G proteins comprised by $G\alpha$, $G\beta$, and $G\gamma$ subunits, transducing extracellular stimuli into intracellular signals by promoting the exchange of $G\alpha$ bound GDP with GTP, which, in turn, results in subunit dissociation and second messenger signaling cascades within cells. GPCRs are divided into four subclasses: $G_{i/o}$, $G_{q/11}$, G_s, and $G_{12/13}$, each interacting uniquely with second messengers, resulting in receptor-type specific cellular responses. Up- or down-regulation of functional molecules, specific for each signaling cascade, causes spatial and temporal events that lead to ordered and dynamic redistribution of intracellular contents.

Functional biochemical and cell-based assays are widely used in GPCR research. In addition to detecting ligand binding, they can also be used to investigate the ligand efficacy to induce cell signaling and biased signaling.[3] Functional assays detect the presence of second messengers or other downstream molecules in response to receptor activation.[4] As different receptor subtypes regulate these events in a subtype-specific manner,[5] any given assay detects signaling events only when signaling occurs via the pathway toward which the assay is sensitive. Also, even though some assays can be designed to be sensitive toward multiple pathways, for example, by creating

artificial signaling pathways in cells, these modifications can alter receptor function.[6] Many assays also provide only end-point data or require addition of labeling compounds, or both.[4] Recently, real-time label-free techniques have emerged as noninvasive alternatives for GPCR signaling pathway detection in cells.[7−10] By immobilizing living cells on sensor surfaces, the measured label-free signals originate from intracellular changes in close proximity to the sensor surface as a response to receptor activation.[11] The advantages of real-time label-free methods are that they provide real-time data and they do not require labels, which can alter cell functions[12] or affect sample properties,[13] to produce a signal output. Also, receptors can be monitored in their native state without altering their functionality. Real-time label-free cell assays are, therefore, excellent for probing new drug candidates as they are not biased to any GPCR subclass. Common methods used in real-time label-free cell measurements include electrical impedance and optical methods such as biolayer interferometry, resonant waveguide grating (RWG), and surface plasmon resonance (SPR).[7−10,14,15] RWG and SPR function by measuring refractive index (RI) changes within the evanescent field, usually reaching a distance of 100−400 nm from the sensor surface. In practice, RI changes are governed by mass
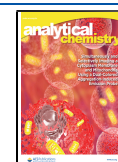
alterations and, when cells are immobilized on the sensors, the RI is dominated by the immense amount of cellular mass[16] and redistribution of intracellular contents upon receptor activation.[8,17]

Many GPCR subtypes induce cell responses that are detectable by label-free techniques, and the spatial and temporal events occurring within cells translate to characteristic real-time label-free signal profiles for different GPCR subtypes.[14,15,18] So far, there is convincing evidence that the G_s pathway can be distinguished from other pathways by simply observing the real-time label-free responses of agonist-stimulated cells.[7,14,19,20] Attempts have been made toward also separating the G_q, G_i, and $G_{12/13}$ pathways, but the results have not been conclusive.[9,10,14,15,18,21,22] Even though real-time label-free systems have shown their potential as the "swiss army knife" method for detecting responses initiated by any of the G protein-coupled pathways mediated by different GPCRs, they have not yet been successful in correlating the label-free signal output to specific receptor subtype in a simple single-step analysis setup. Instead, a multiple-step analysis with additional antagonists or other response modifying agents have to be used to associate label-free signal responses to a specific G protein-coupled signaling cascade.[10,21−24] This can be problematic if antagonists do not exist for a receptor and especially problematic for orphan receptors with no known ligands. Lastly, treating cells to silence or otherwise alter G protein coupling may redirect signaling pathways from their original activity to alternative cascades.[25]

In this study, we show that more information-rich real-time label-free signal profiles for different GPCR signaling pathways can be derived from the analysis of signal responses obtained using a continuous angular-scanning SPR method. The measurements are conducted in a single-step analysis setup without the need for prior cell treatments, use of antagonists, or pathway-modulating compounds. Different cell lines expressing GPCRs coupled to $G\alpha_s$, $G\alpha_i$, or $G\alpha_q$ were used as model systems. Following the agonist-induced receptor stimulation, we show that the single-parameter SPR signal profiles for G_s and G_q pathways correlate well with those from previous studies using similar label-free methods. We then present how GPCR pathway analysis comparing multiple SPR parameters provides label-free signal profiles that exhibit improved specificity to the GPCR signaling via G_q-, G_s-, and G_i-coupled pathways.

■ MATERIALS AND METHODS

Cell Immobilization on Sensors. Cells were immobilized on the sensors, as described previously.[16] Briefly, cells were first detached from 80−90% confluent cell culture vessels using TrypLE Express (12604, Thermo Fisher) or 0.05% trypsin-ethylenediaminetetraacetic acid (EDTA) (15400, Thermo Fisher) and resuspended into a complete growth medium at the desired concentration. Cell suspensions were then carefully pipetted over the sensors. For HeLa cells, sensors were first coated with human fibronectin (FC010, Sigma-Aldrich), whereas for CHO-K1 and A431 cells, uncoated sensors were used. Sensors with cells were cultured at 37 °C in 5% CO_2 for 48−96 h until ∼100% confluent. The culture medium was renewed once after 24 h of incubation.

Surface Plasmon Resonance (SPR) Measurements. The SPR experiments were performed using an MP-SPR Navi instrument (Bionavis Ltd.). Prior to the SPR experiments, flow channels and all fluidic paths were primed with the assay buffer, and the flow channels were heated to 37 °C (±0.1 °C). The used buffer was chosen according to the basal media used for cell cultures. For CHO-K1 cells, Dulbecco's modified Eagle's medium (DMEM)/nutrient mixture F-12 Ham containing 15 mM N-(2-hydroxyethyl)piperazine-N'-ethanesulfonic acid (HEPES) supplemented with 1% penicillin−streptomycin (PS) was used. For A431 and HeLa cells, DMEM containing 1 g/L D-glucose and 25 mM HEPES supplemented with 1% PS was used. Before inserting the sensors into the SPR device, the sensors on which the cells were cultured were examined under a light microscope to confirm sufficient cell confluence, morphology, and monolayer integrity. A flow rate of 20−30 μL/min was used and an angle range of 59−76° was scanned continuously with a temporal resolution of approximately 6.5 s. Once the signal reached a stable baseline, samples were injected for 15 min, after which buffer flow resumed. A reference sample with matching composition but without active compounds was always injected to the second channel concurrently with the test sample. At the end of the experiments, cell sensors were treated with trypan blue and observed under a microscope for viability.

Resonant Waveguide Grating (RWG) Measurements. RWG measurements were performed using an EnSpire multimode reader (PerkinElmer). Before experiments, media in the well plates were replaced with the assay buffer. The plate was then inserted into the device and equilibrated for 1 h, after which a baseline read was taken for 30 min. Next, samples were introduced to cells by ejecting the plate and pipetting sample solutions to the wells. Three wells were used as controls, where only buffer was added. The plate was then inserted quickly back into the device and real-time measurement was started. The wavelength shifts in all of the wells from one quarter of a 96-well plate were detected simultaneously. The maximum temporal resolution of 15 s was used. Experiments were performed at 26 °C (±3 °C). Assay buffer was DMEM containing 4.5 g/L D-glucose supplemented with 1% PS and 10 mM HEPES. All samples were measured in three replicates.

Data Analysis. SPR data were extracted using the SPR Navi Data viewer software (v. 4.3.3) (Bionavis Ltd.). The moment of sample injection was selected as a zero time point, where time and SPR response were set as zero. Further data analysis was done using OriginPro (v. b9.5.5.409) (OriginLab Corporation, Northampton, MA) and GraphPad Prism (v. 8.4.1) (GraphPad Software, San Diego, CA). All real-time cell responses were background corrected by subtracting any bulk response caused by the reference sample in the control channel from the response of the sample channel. The area under the curve (AUC) was used to plot concentration-response curves from which EC_{50} values were determined using nonlinear regression. AUC was calculated from T_0 to T_{end}, where T_0 is defined as the moment immediately before the sample enters the measurement channel and T_{end} is the SPR signal at the time when sample injection is ended. Any negative values were neglected when calculating AUC values.

RWG data were extracted using EnSpire Manager software (v. 4.1) (PerkinElmer). All data analysis was done using OriginPro and GraphPad Prism. The average response of three control wells was subtracted from the sample well responses and real-time data were plotted as picometers (pm) against time.

RESULTS

The cell lines used in this study express different GPCRs, which are coupled to three different G proteins: G_i, G_q, and G_s, each initiating their respective cell signaling pathways. With A431 cells, the agonists used were bradykinin and epinephrine, which bind to bradykinin B_2 and $ß_2$-adrenoceptors, activating G_q and G_s pathways, respectively. With HeLa and CHO-K1 cells expressing the histamine H_3 receptor hH$_3$R-445 (CHO-K1-hH$_3$R), histamine was used, which binds to histamine H_1 and H_3 receptors, activating G_q and G_i pathways in these cells, respectively. The other ligands and their targets used in this study are shown in Table 1.

Table 1. List of Ligands and Cell Lines Used in This Study

ligand	agonist/ antagonist	target receptor (pathway)	cell line[a]
bradykinin	agonist	bradykinin B_2 (G_q)	A431
epinephrine	agonist	$ß_2$-adrenoceptor (G_s)	A431
histamine	agonist	histamine H_1 (G_q), histamine H_3 (G_i)	HeLa, CHO-K1-hH$_3$R, CHO-K1
mepyramine	antagonist	histamine H_1 (G_q)	HeLa, CHO-K1-hH$_3$R
ranitidine	antagonist	histamine H_2	HeLa, CHO-K1-hH$_3$R
thioperamide	antagonist	histamine H_3 (G_i)/H$_4$	HeLa, CHO-K1-hH$_3$R
JNJ-7777120	antagonist	histamine H_4	HeLa, CHO-K1-hH$_3$R

[a]A431 = human epithelial squamous carcinoma cell line, HeLa = human epithelial cervical adenocarcinoma cell line, CHO-K1 = PathHunter Chinese hamster ovary (CHO-K1) parental cell line, and CHO-K1-hH$_3$R = CHO-K1 cell line expressing the hH$_3$R-445.

Cell Immobilization on Sensors. All cell lines were successfully immobilized on the SPR sensors and showed near fully confluent cell monolayers under the microscope at the end of the incubation periods. CHO-K1 and A431 cells attached to the gold-coated sensors and retained uniform monolayers and cell viability, even after an extended time in the SPR instrument during the experiments (Figure S1A,B), whereas Hela cells remained fully attached on sensors only when a fibronectin coating was applied (Figure S1C,D).

The presence of cell monolayers was also evident from the full SPR curves (Figure S2). The SPR sensors without cells show a sharp and definable total internal reflection (TIR) region at an angle around 61°, and the position of the main SPR peak or peak angular position (PAP) at an angle around 66°. Noticeable changes in TIR and PAP were observed with the cell monolayers present on the sensors. The exact shape and the position of the TIR region and the PAP were somewhat dependent on the cell type. In general, cells caused the TIR region to become less defined with an angular position at around 63°, while the PAP increased to 68−69°.

SPR Peak Angular Position (PAP) Responses During GPCR Activation. Figure 1 shows the SPR PAP responses against time during the stimulation of A431 cells with different concentrations of epinephrine and bradykinin, and during the stimulation of CHO-K1-hH$_3$R and HeLa cells with different concentrations of histamine. All agonists caused immediate responses in PAP. A431 cells with bradykinin and epinephrine showed unique real-time signal profiles: bradykinin caused a rapid signal increase, reaching a maximal signal shift close to 600 millidegrees within 2 min with the three highest concentrations, after which the signals started to quickly decrease, reaching close to the initial values during the 15 min sample injections (Figure 1A). Epinephrine, on the contrary,
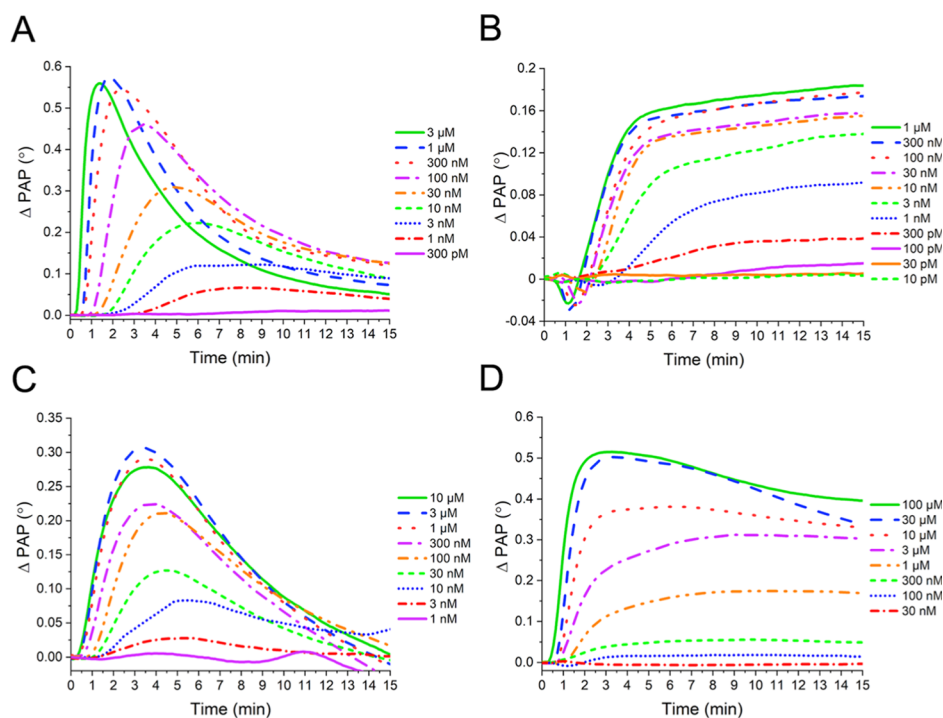

Figure 1. Representative surface plasmon resonance (SPR) peak angular position (PAP) responses to G protein-coupled receptor activation. Responses to different concentrations of bradykinin (A) and epinephrine (B) with A431 cells and to different concentrations of histamine with CHO-K1-hH$_3$R cells (C) and HeLa cells (D).
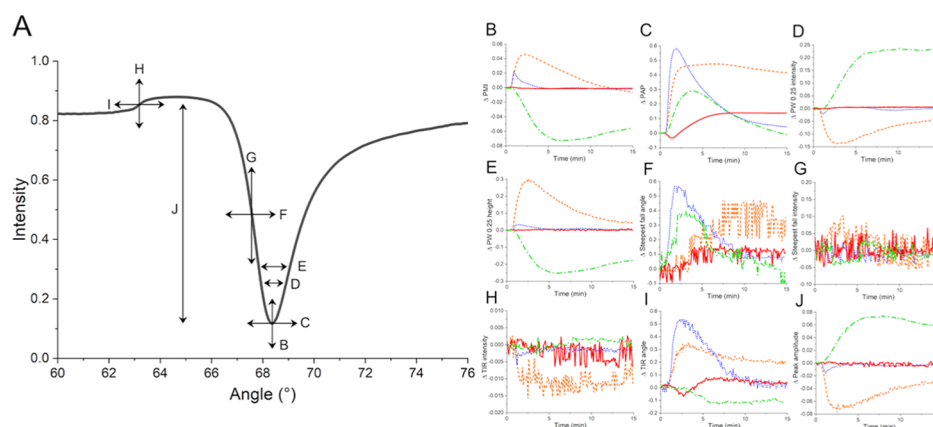
Figure 2. Representative real-time responses of additional surface plasmon resonance (SPR) parameters. (A) Representation on how different SPR parameters relate to the measured full SPR curve. (B−J) Real-time responses of peak minimum intensity (B), peak angular position (C), peak width at 0.25 intensity (D), peak width at 0.25 peak amplitude (E), steepest fall angle (F), steepest fall intensity (G), total internal reflection (TIR) intensity (H), TIR angle (I), and peak amplitude (J) during sample injections of histamine with HeLa cells (orange dashed lines), bradykinin with A431 cells (blue dotted lines), epinephrine with A431 cells (red solid lines), and histamine with CHO-K1-hH$_3$R cells (green dashed and dotted lines). All signal response curves are for agonists at concentrations well above their EC$_{50}$ values.

caused a small initial decrease in the PAP response (Figure 1B). However, this was reversed within 60−90 s, after which the response showed a two-phased signal increase: a rapid rise lasting 2−4 min and a slower rise until the end of the sample injection, reaching a maximal signal shift of around 180 millidegrees at 1 μM. Histamine with CHO-K1-hH$_3$R cells showed very similar PAP response patterns compared to bradykinin with A431 cells: an immediate signal increase, followed by a gradual decrease after reaching a maximal signal shift of around 300 millidegrees with the three highest concentrations (Figure 1C). Histamine with HeLa cells showed PAP response characteristics from both bradykinin and epinephrine with A431 cells: the signal increased immediately, reaching a maximum shift of 520 millidegrees at 100 μM and showing only slight or no signal decrease during sample injections (Figure 1D). The PAP response curves were used to calculate the AUC values, whereby concentration-response curves were plotted and the EC$_{50}$ values were subsequently calculated for all agonists (Figure S3). Average pEC$_{50}$ values ($\pm$standard error of mean (SEM)) of 8.0 $\pm$ 0.09 (n = 3) for bradykinin and 8.9 $\pm$ 0.13 (n = 3) for epinephrine were obtained, while the pEC$_{50}$ values ($\pm$SEM) for histamine with CHO-K1-hH$_3$R cells was 6.9 $\pm$ 0.29 (n = 3) and 5.7 $\pm$ 0.06 (n = 3) with HeLa cells.

To observe cell responses to ligand removal, SPR measurements were allowed to continue after sample injections ended. With all agonists, PAP signals returned to their initial values, or very close to the initial values (data not shown). Also, the cells remained responsive to repeated stimulation with the same ligand, except with the HeLa cells, where a second histamine stimulation showed a clearly desensitized response even after 135 min washout between the sample injections (Figure S4).

Pathway Analysis. In addition to PAP, continuous recording of the full SPR curve allows monitoring of several other SPR signal responses (Figure 2A). We plotted eight additional SPR parameters: peak minimum intensity (PMI), peak amplitude, peak width at 0.25 intensity, peak width at 0.25 peak amplitude, TIR angle, TIR intensity, steepest fall intensity, and steepest fall angle for all agonists at concentrations above their EC$_{50}$ values (Figure 2B−J). Many of these signal responses exhibited consistent and pathway-

dependent changes. To further evaluate these additional parameters, rather than observing them one by one, we plotted all of the additional parameters against PAP responses (Figure S5). Four of these plots showed potential for pathway separation. However, the PMI against PAP exhibited particularly promising pathway specificity and was, therefore, chosen for further analysis (parameters B and C from Figure 2). PMI is the measure of the dynamic intensity shift of the peak minimum of the full SPR curve (Figure 2A). Figure 2B shows a comparison of representative PMI responses for all agonists. The observed PMI signals can be divided into two distinct response profiles: increasing or decreasing below the baseline. Histamine with HeLa cells and bradykinin with A431 cells show an increase in PMI responses, while histamine with CHO-K1-hH$_3$R cells and epinephrine with A431 cells show a decrease in PMI. The PMI profile for bradykinin closely resembles the bradykinin PAP profile: signal reaches its peak maximum in less than 60 s and then exhibits a quick return to initial baseline (compare Figure 2B and Figure 2C). Histamine PMI response with HeLa cells resembles the bradykinin PMI response profile, except that the signal shows slightly slower kinetics, reaching the peak after 2 min and declining back to the initial value only toward the end of sample injection. Histamine with CHO-K1-hH$_3$R cells and epinephrine with A431 cells both show similar PMI response profiles, with only a decline in the signal, reaching the minimum within 5−6 min. However, the decrease in PMI response for epinephrine with A431 cells was negligible compared to histamine with CHO-K1-hH$_3$R cells and, therefore, not visible in Figure 2B. The PMI response peaks for histamine with HeLa and CHO-K1-hH$_3$R cells reached maximum and minimum PMI shifts of 0.045 and −0.073, respectively. Bradykinin and epinephrine showed much subtler responses with maximum and minimum PMI shifts of 0.025 and −0.0014, respectively.

Figure 3 shows the two-parameter PMI-PAP response profiles for all agonists with all cell lines at agonist concentrations that induce maximum signal responses. From this graph, it is clear that each GPCR signaling pathway produces an unambiguously distinguishable pattern on this two-dimensional angle-intensity graph. Both compounds activating G$_q$-coupled receptors in different cellular contexts,
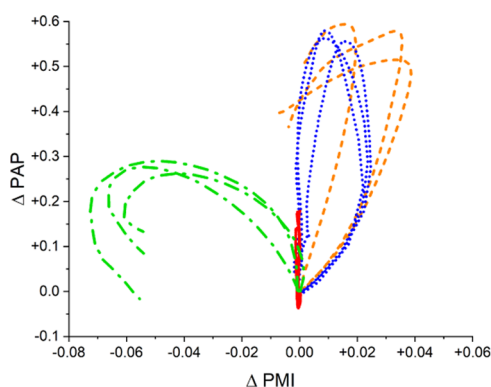
Figure 3. Two-parameter surface plasmon resonance (SPR) response profiles. Peak angular position (PAP) responses are plotted against peak minimum intensity (PMI) responses for histamine with CHO-K1-hH$_3$R cells (green lines with dashes and dots, G$_i$), epinephrine with A431 cells (red solid lines, G$_s$), bradykinin with A431 cells (blue lines with dots, G$_q$), and histamine with HeLa cells (orange lines with dashes, G$_q$). For each response profile, three independent measurements with agonists at concentrations inducing maximum PAP responses are shown.

lean to the right and create a loop shape. The G$_i$-coupled receptor activation creates a similar loop but leans strongly to the left, while the G$_s$-coupled receptor activation draws a straight line across the y-axis.

SPR Responses Originate from Receptor Activation. To confirm that the measured SPR signals originate from the cell responses specific to GPCRs, we used a range of histamine receptor antagonists, G protein inhibitors, and parental CHO-K1 cells that were not transfected with the hH$_3$R-445. As expected, parental CHO-K1 cells did not show any response when exposed to 300 nM histamine (Figure S6A). Histamine H$_1$ receptor antagonist mepyramine at 1 μM, histamine H$_2$ receptor antagonist ranitidine at 10 μM, or histamine H$_4$ receptor antagonist JNJ-7777120 (JNJ) at 1 μM did not attenuate CHO-K1-hH$_3$R cell responses to 300 nM histamine (Figure S6B). On the contrary, thioperamide, an H$_3$/H$_4$ antagonist at 1 μM, given concurrently with 300 nM histamine, decreased the PAP AUC to around 10%, compared to histamine alone. Furthermore, overnight treatment with 1 μM YM-254890 (YM), a peptide inhibiting G$_q$-coupled receptor signaling, did not inhibit cell response to histamine, whereas overnight treatment with 100 ng/mL pertussis toxin (PTX), a G$_i$ inhibitor, completely abolished the response. With HeLa cells, which endogenously express G$_q$-coupled histamine H$_1$ receptors, no effect was seen when cells were stimulated with 10 μM histamine concurrently with 10 μM ranitidine, 1 μM thioperamide, and 1 μM JNJ or after cells were treated overnight with 100 ng/mL PTX (Figure S6C). However, with concurrent exposure to 1 μM mepyramine, the PAP AUC decreased to around 7% of that with histamine alone and to around 6% after 15 min treatment with 10 μM YM.

Comparison of SPR PAP Responses with RWG Responses. We compared the SPR PAP responses with responses measured using RWG. Results from both systems were well in accordance with each other (Figures 4A and S7). The overall shapes of the RWG and SPR response curves follow closely similar patterns. However, with bradykinin-stimulated A431 cells, the main response peaks in RWG always occurred at earlier time points and saturated at lower agonist concentrations compared to SPR. This is more pronounced
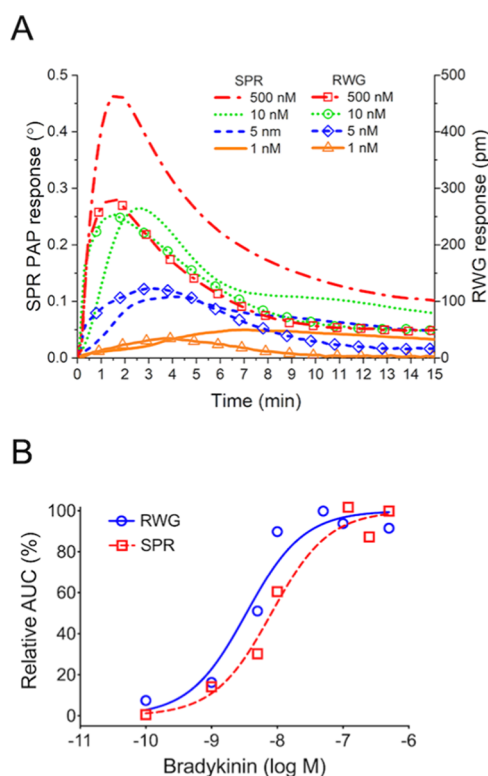

Figure 4. Comparison between surface plasmon resonance (SPR) and resonant waveguide grating (RWG). (A) Representative real-time responses to different concentrations of bradykinin with A431 cells on sensors. Concentrations are: 1, 5, 10, and 500 nM with orange solid lines, blue dashed lines, green dotted lines, and red dashed and dotted lines, respectively. Lines without markers are SPR responses and lines with markers are RWG responses. Left y-axis is SPR PAP response and right y-axis RWG response. (B) Representative concentration-response curves for bradykinin determined from the area under the curve (AUC) of SPR PAP and RWG responses. RWG responses are the solid blue line with circles and SPR PAP responses are the dashed red line with squares.

with the highest concentration, where the initial signal shift is rapid and strong (Figure 4A). These differences are most likely a consequence of sample handling. With RWG, measurement is halted during sample addition and initial cell response is therefore lost, whereas with SPR, measurement is never interrupted.

Despite these differences, the concentration-response curves plotted for RWG and SPR responses compare closely with each other (Figure 4B). The EC$_{50}$ value for bradykinin-stimulated A431 cells calculated from AUC of the RWG responses was around 3 nM, which is close to the value of 10 nM obtained using the SPR responses. The slightly lower EC$_{50}$ value with RWG is probably a consequence of the loss of initial temporal resolution.

■ DISCUSSION

The sensitivity of real-time label-free methods allows detecting very small mass alterations originating from localized cellular mass rearrangement, such as changes in cell morphology or even intracellular mass movements.[26] This mass sensing property makes real-time label-free cell assays inherently different from traditional functional cell assays, as all cell events occurring within the detection area are monitored instead of only a single specific predetermined cellular

response. This makes these methods a great choice for measuring a number of different cell responses, such as GPCR cell signaling. GPCR pathway analysis with label-free methods is based on the ability of these techniques to translate the spatial and temporal mass redistribution within cells into real-time signals.[9,14,15] As the activated GPCR signaling pathways within cells can lead to either an increase or decrease in relative mass within the label-free sensing area, the label-free responses can also exhibit either a signal increase or decrease from their baseline level, respectively. So far, the label-free identification of G_s and G_q pathways by previous studies have been owed mainly to the uniqueness of the G_s response profile, specifically the initial negative peak but also to the analysis of the time-response signal profile as a whole.[19,27] This time-resolved pathway recognition may work when separating GPCR signaling within the same cellular context, but the same signaling pathways that are activated in different cell types can produce quite different label-free response profiles (compare Figure 1A and Figure 1D).[28] Also, it is interesting to note that much of the data interpretation so far has been focused only on differentiating G_s response from other pathways and on general profiling of G_q and G_i time-response signals. This might be simply due to the time-resolved signal profiles not being sufficiently distinctive to separate G_q and G_i signaling from each other.[10,14,15,29] Furthermore, even though impedance-based methods have shown some potential in distinguishing between these three G protein signaling pathways, the analysis still relies on subtle differences in the kinetic profile of only a single parameter[18] or two closely related parameters.[30] Moreover, results have been variable, where in some cases, depending on the type of instrument and cell lines used, the responses for the same pathway have shown very different response patterns.[9,15,18] To circumvent these drawbacks, an alternative approach, applied in many label-free studies, is to introduce compounds, such as antagonists or inhibitors targeting the signaling proteins, in addition to the agonists to alter or silence label-free responses to separate GPCR signaling pathways.[10,21] However, this introduces more complexity in label-free assays. Because of these challenges, there has not been a well-established label-free method to distinctively distinguish between these three GPCR signaling pathways in a straightforward manner.

Like with other label-free systems, the SPR PAP signals presented in this study reflect the subtle mass redistribution taking place in cells during GPCR activation. In RWG measurements, this is often referred to as dynamic mass redistribution (DMR). However, with the angular-scanning SPR, we are not limited only to measuring the PAP responses. Instead, much more information-rich label-free signals can be extracted from the full SPR curves (Figure 2A). While it has been demonstrated that more than one parameter can also be measured with angular-scanning RWG,[17] further pathway analysis using additional parameters has not been explored. We have previously demonstrated how the continuously recorded full SPR curve can provide deeper label-free analysis of cellular responses.[31] Measuring the dynamic responses of the full SPR curves during the activation of GPCRs revealed that, in addition to PAP, at least five other label-free parameters exhibited time-dependent responses that might be used for pathway separation (Figure 2B,D,E,I,J). Of these, further analysis indicated that the PMI signals showed the best separation of GPCR subtypes (Figures 3 and S5). Unlike the PAP responses, the PMI signals are not sensitive directly to the

amount of mass within the evanescent field. Instead, PMI is affected by the amount of light that is reflected back at the SPR coupling angle and is sensitive to any absorbing or scattering surfaces within the sensing depth. With cell assays, this means that any event where the total mass does not necessarily change, but the surface area of scattering interfaces that the surface plasmons encounter increases or decreases, changes in PMI occur. This type of scatter-inducing changes in cells have been described earlier and were associated mainly with morphological changes in the cell membrane.[32] Of course, other cellular processes can be expected to also influence surface plasmon scattering.

When looking at the PMI changes caused by the activation of different GPCRs, it is evident that, like the PAP responses presented here and other label-free signal profiles reported by other groups, the PMI responses also display complex kinetic profiles, indicating that PMI responses are sensitive to the unique cellular processes initiated by different active G protein subtypes. What is more interesting, compared to the PAP profiles, is that the SPR PMI responses seem to exhibit higher signal pattern specificity for each pathway: increase, decrease, and only a minor negative change in PMI responses for G_q, G_i, and G_s pathways, respectively (Figure 2B). Also, it seems that the PMI responses are not as sensitive to the cellular context as PAP responses, as evident from the more apparent correlation of the PMI profiles associated to the G_q signaling pathway, demonstrated by bradykinin-stimulated A431 cells and histamine-stimulated HeLa cells (compare Figure 2B and Figure 2C). Because of these unique PMI responses, the three GPCR signaling pathways are, in this case, recognizable solely from the PMI profiles. However, by observing PAP and PMI together, stronger correlation between SPR response patterns and GPCR signaling pathways, especially across different cellular backgrounds, should be achieved (Figure 3). However, further experiments, collecting data from broader selection of cell lines, receptor types, and a range of different ligands targeting these receptors, are warranted to validate the robustness of this multiple SPR parameter analysis as a method for unambiguous GPCR pathway recognition. Also, the cellular context for measuring the $G_{12/13}$ pathway with angular-scanning SPR should be investigated to establish the label-free signal profile for this pathway.

Because SPR has not been widely used for GPCR signal profiling, comparison with more established label-free systems is warranted. The observed PAP time-response profiles for G_q and G_s signaling pathways are in good accordance with the results from other groups using similar optical label-free systems: activation of the G_q signaling pathway in A431 cells shows a two-phased overall response profile with a rapid initial signal increase followed by a decreasing signal (Figure 1A),[14] while the same pathway in HeLa cells shows only an increasing overall signal profile with little or no signal decrease (Figure 1D).[8,28] In addition to differences in the G_q response profiles under a different cellular context, some G_q signal profile differences in the same cell type can also be observed between different studies: Lu et al.[8] reported a triphasic early G_q signal increase with HeLa cells using both SPR and impedance methods, while results by Yu et al.[15] using an impedance method and by Deng et al.[28] using RWG showed, similarly to our results, only a single-phased early signal increase. For the G_s pathway, the signal profiles seem to be fairly uniform even across different label-free techniques and cell types.[7,9,14] To the best of our knowledge, real-time label-free G_s signaling

pathway responses are not previously reported using SPR. Our results show that the SPR responses during G_s activation are very well in line with other label-free methods, showing an immediate but transient signal decrease followed by a two-phased increase (Figure 1B). There have been previous attempts to also profile the G_i signaling pathway using RWG and impedance methods, and even though results have not been conclusive, all cell responses attributed to the G_i signaling pathway have shown signal profiles with increasing signal responses,[9,10,14,15,18,21,22,29] and our results support these previous observations (Figure 1C). Lastly, the EC_{50} values obtained for histamine with HeLa cells and for epinephrine and bradykinin with A431 cells are well in line with previously reported values measured with optical label-free methods.[8,27,33] However, it is worth noting that the EC_{50} value for histamine with CHO-K1-hH$_3$R cells shows greater variation than the other agonist-receptor pairs (Figure S3C). This is likely due to loss of receptor expression with cells having higher passage numbers, resulting in lowered SPR responses (Figure S8).

We also compared the SPR technique directly with RWG. Parallel measurements showed that the SPR and RWG responses correlated closely. PAP responses from SPR and RWG responses showed matching G_q and G_s signal profiles with A431 cells and comparable EC_{50} values for bradykinin (Figures 4 and S7). An advantage of SPR over RWG is that information on receptor activation is obtained in dynamic flow conditions with no delay in measured responses. This was observed as better SPR sensitivity to higher bradykinin concentrations with A431 cells (Figure 4).

The observations presented in this study, and results reported in previous studies by other groups, indicate that while the label-free signal profiles depend mainly on the GPCR signaling pathway, they are also dependent on the cellular context and the label-free techniques used as these methods are sensitive to a variety of assay conditions. Therefore, other factors besides GPCR signaling pathways can play an important role in the observed label-free signal responses and, therefore, using the time-resolved single-parameter signal profile analysis alone for interpreting GPCR signaling pathways presents some uncertainty. This underlies the need for more advanced signal analysis methods for an unambiguous GPCR pathway recognition by real-time label-free methods, such as using multiple label-free parameters concurrently.

CONCLUSIONS

We have demonstrated how the continuous angular-scanning SPR can be used to recognize and separate GPCRs into subtype-specific G_q, G_s, and G_i signaling pathways. Label-free detection occurs in real-time and pathway separation is achieved by measuring multiple SPR parameters during cell exposure to receptor agonists only. No concurrent antagonists or other response modulating agents are required. We measured the signaling profiles for the G_q and G_i pathways and, to our knowledge, for the first time with SPR for the G_s pathway. We showed that by combining different label-free parameters (in this study the dynamic angular (PAP) and intensity (PMI) shifts of the full SPR curve peaks), each subtype-specific GPCR signaling pathway creates a unique label-free response profile, from which GPCR signaling routes can be identified. To date, the focus in label-free GPCR profiling has remained on signal deconvolution in the presence of response modulating compounds and high-throughput analysis. We believe that the results presented in this study

demonstrate that the strength of real-time label-free methods lies in fact in the high information content that these techniques are capable of and, therefore, need for more advanced signal analysis methods is justified.

ASSOCIATED CONTENT

Ⓢ Supporting Information

The Supporting Information is available free of charge at https://pubs.acs.org/doi/10.1021/acs.analchem.0c02652.

Materials and methods in detail, SPR cell sensor images, full SPR curves, concentration-response curves, desensitization experiments, two-parameter plots, control SPR experiments, and SPR epinephrine response comparison with RWG and CHO-K1-hH$_3$R cell passage effect to SPR signal (PDF)

AUTHOR INFORMATION

Corresponding Authors

Teemu Suutari — *Drug Research Program, Division of Pharmaceutical Biosciences, Faculty of Pharmacy, University of Helsinki, 00014 Helsinki, Finland; Division of BioAnalytical Chemistry, Amsterdam Institute for Medicines, Molecules and Systems, Vrije Universiteit Amsterdam, 1081 HZ Amsterdam, The Netherlands;* ⓘ orcid.org/0000-0002-7375-8678; Email: teemu.suutari@helsinki.fi

Tapani Viitala — *Drug Research Program, Division of Pharmaceutical Biosciences, Faculty of Pharmacy and Drug Research Program, Division of Pharmaceutical Chemistry and Technology, Faculty of Pharmacy, University of Helsinki, 00014 Helsinki, Finland;* ⓘ orcid.org/0000-0001-9074-9450; Email: tapani.viitala@helsinki.fi

Authors

Sabrina N. Rahman — *Division of Medicinal Chemistry, Amsterdam Institute for Medicines, Molecules and Systems, Faculty of Science, Vrije Universiteit Amsterdam, 1081 HZ Amsterdam, The Netherlands*

Henry F. Vischer — *Division of Medicinal Chemistry, Amsterdam Institute for Medicines, Molecules and Systems, Faculty of Science, Vrije Universiteit Amsterdam, 1081 HZ Amsterdam, The Netherlands;* ⓘ orcid.org/0000-0002-0184-6337

Dick van Iperen — *Precision Mechanics and Engineering Beta, Vrije Universiteit Amsterdam, 1081 HV Amsterdam, The Netherlands*

Arto Merivaara — *Drug Research Program, Division of Pharmaceutical Biosciences, Faculty of Pharmacy, University of Helsinki, 00014 Helsinki, Finland*

Marjo Yliperttula — *Drug Research Program, Division of Pharmaceutical Biosciences, Faculty of Pharmacy, University of Helsinki, 00014 Helsinki, Finland*

Rob Leurs — *Division of Medicinal Chemistry, Amsterdam Institute for Medicines, Molecules and Systems, Faculty of Science, Vrije Universiteit Amsterdam, 1081 HZ Amsterdam, The Netherlands;* ⓘ orcid.org/0000-0003-1354-2848

Jeroen Kool — *Division of BioAnalytical Chemistry, Amsterdam Institute for Medicines, Molecules and Systems, Vrije Universiteit Amsterdam, 1081 HZ Amsterdam, The Netherlands; Centre for Analytical Sciences Amsterdam (CASA), 1098 XH Amsterdam, The Netherlands;* ⓘ orcid.org/0000-0002-0011-5612

Complete contact information is available at:
https://pubs.acs.org/10.1021/acs.analchem.0c02652

Notes

The authors declare no competing financial interest.

REFERENCES

(1) Sriram, K.; Insel, P. A. *Mol. Pharmacol.* **2018**, *93*, 251−258.

(2) Hauser, A. S.; Attwood, M. M.; Rask-Andersen, M.; Schiöth, H. B.; Gloriam, D. E. *Nat. Rev. Drug Discovery* **2017**, *16*, 829.

(3) Kenakin, T.; Christopoulos, A. *Nat. Rev. Drug Discovery* **2013**, *12*, 205−216.

(4) Zhang, R.; Xie, X. *Acta Pharmacol. Sin.* **2012**, *33*, 372.

(5) Neves, S. R.; Ram, P. T.; Iyengar, R. *Science* **2002**, *296*, 1636−1639.

(6) Kostenis, E. *Trends Pharmacol. Sci.* **2001**, *22*, 560−564.

(7) Verzijl, D.; Riedl, T.; Parren, P. W. H. I.; Gerritsen, A. F. *Biosens. Bioelectron.* **2017**, *87*, 388−395.

(8) Lu, J.; Yang, Y.; Wang, W.; Li, J.; Tao, N.; Wang, S. *Anal. Chem.* **2016**, *88*, 11498−11503.

(9) Stallaert, W.; Dorn, J. F.; van der Westhuizen, E.; Audet, M.; Bouvier, M. *PLoS One* **2012**, *7*, No. e29420.

(10) Schröder, R.; Janssen, N.; Schmidt, J.; Kebig, A.; Merten, N.; Hennen, S.; Müller, A.; Blättermann, S.; Mohr-Andrä, M.; Zahn, S.; Wenzel, J.; Smith, N. J.; Gomeza, J.; Drewke, C.; Milligan, G.; Mohr, K.; Kostenis, E. *Nat. Biotechnol.* **2010**, *28*, 943−949.

(11) Fang, Y.; Frutos, A. G.; Verklereen, R. *Comb. Chem. High Throughput Screening* **2008**, *11*, 357−369.

(12) Hu, H.; Deng, H.; Fang, Y. *PLoS One* **2012**, *7*, No. e34934.

(13) Baker, J. G.; Middleton, R.; Adams, L.; May, L. T.; Briddon, S. J.; Kellam, B.; Hill, S. J. *Br. J. Pharmacol.* **2010**, *159*, 772−786.

(14) Fang, Y.; Li, G.; Ferrie, A. M. *J. Pharmacol. Toxicol. Methods* **2007**, *55*, 314−322.

(15) Yu, N.; Atienza, J. M.; Bernard, J.; Blanc, S.; Zhu, J.; Wang, X.; Xu, X.; Abassi, Y. A. *Anal. Chem.* **2006**, *78*, 35−43.

(16) Suutari, T.; Silen, T.; Sen Karaman, D.; Saari, H.; Desai, D.; Kerkelä, E.; Laitinen, S.; Hanzlikova, M.; Rosenholm, J. M.; Yliperttula, M.; Viitala, T. *Small* **2016**, *12*, 6289−6300.

(17) Fang, Y.; Ferrie, A. M.; Fontaine, N. H.; Mauro, J.; Balakrishnan, J. *Biophys. J.* **2006**, *91*, 1925−1940.

(18) Verdonk, E.; Johnson, K.; McGuinness, R.; Leung, G.; Chen, Y.-W.; Tang, H. R.; Michelotti, J. M.; Liu, V. F. *ASSAY Drug Dev. Technol.* **2006**, *4*, 609−619.

(19) Fang, Y.; Frutos, A. G.; Randle, D. H.; Tran, E. High-Throughput High-Information Content Label-Free Cell Biology Screening Methods. U.S. Patent US8,846,5752014.

(20) Ferrie, A. M.; Wang, C.; Deng, H.; Fang, Y. *Integr. Biol.* **2013**, *5*, 1253−1261.

(21) Ferrie, A. M.; Sun, H.; Zaytseva, N.; Fang, Y. *Sci. Rep.* **2015**, *4*, No. 3828.

(22) Schröder, R.; Schmidt, J.; Blättermann, S.; Peters, L.; Janssen, N.; Grundmann, M.; Seemann, W.; Kaufel, D.; Merten, N.; Drewke, C.; Gomeza, J.; Milligan, G.; Mohr, K.; Kostenis, E. *Nat. Protoc.* **2011**, *6*, 1748−1760.

(23) Fang, Y.; Gao, Y. A.; Tran, E. Label-Free Methods Using a Resonant Waveguide Grating Biosensor to Determine GPCR Signaling Pathways. U.S. Patent US8,426,1482013.

(24) Deng, H.; Wang, C.; Su, M.; Fang, Y. *Anal. Chem.* **2012**, *84*, 8232−8239.

(25) Luttrell, L. M.; Wang, J.; Plouffe, B.; Smith, J. S.; Yamani, L.; Kaur, S.; Jean-Charles, P.-Y.; Gauthier, C.; Lee, M.-H.; Pani, B.; Kim, J.; Ahn, S.; Rajagopal, S.; Reiter, E.; Bouvier, M.; Shenoy, S. K.; Laporte, S. A.; Rockman, H. A.; Lefkowitz, R. J. *Sci. Signaling* **2018**, *11*, No. eaat7650.

(26) Yanase, Y.; Suzuki, H.; Tsutsui, T.; Hiragun, T.; Kameyoshi, Y.; Hide, M. *Biosens. Bioelectron.* **2007**, *22*, 1081−1086.

(27) Tran, E.; Fang, Y. *J. Biomol. Screening* **2008**, *13*, 975−985.

(28) Deng, H.; Sun, H.; Fang, Y. *J. Pharmacol. Toxicol. Methods* **2013**, *68*, 323−333.

(29) Grundmann, M.; Merten, N.; Malfacini, D.; Inoue, A.; Preis, P.; Simon, K.; Rüttiger, N.; Ziegler, N.; Benkel, T.; Schmitt, N. K.; Ishida, S.; Müller, I.; Reher, R.; Kawakami, K.; Inoue, A.; Rick, U.; Kühl, T.; Imhof, D.; Aoki, J.; König, G. M.; Hoffmann, C.; Gomeza, J.; Wess, J.; Kostenis, E. *Nat. Commun.* **2018**, *9*, No. 341.

(30) Leung, G.; Tang, H. R.; McGuinness, R.; Verdonk, E.; Michelotti, J. M.; Liu, V. F. *J. Assoc. Lab. Autom.* **2005**, *10*, 258−269.

(31) Viitala, T.; Granqvist, N.; Hallila, S.; Raviña, M.; Yliperttula, M. *PLoS One* **2013**, *8*, No. e72192.

(32) Yashunsky, V.; Lirtsman, V.; Golosovsky, M.; Davidov, D.; Aroeti, B. *Biophys. J.* **2010**, *99*, 4028−4036.

(33) Li, G.; Ferrie, A. M.; Fang, Y. *J. Assoc. Lab. Autom.* **2006**, *11*, 181−187.